RSC Advances

ROYAL SOCIETY OF CHEMISTRY

PAPER

View Article Online
View Journal | View Issue

Cite this: *RSC Adv.*, 2026, **16**, 3735

Understanding the influence of group 13 elements on the reactivity of G13–As–Ge imine analogues in 1,3-addition with methyl iodide

Zheng-Feng Zhang[a] and Ming-Der Su *[ab]

Using the M06-2X-D3/def2-TZVP level of theory, we investigated the 1,3-addition reactions of methyl iodide (CH_3I) with a series of heavy imine analogues, **G13**=**As-Rea** (where G13 = group 13 element), which feature a mixed G13–As–Ge backbone. Theoretical evidence reveals that the bonding character of the G13=As moiety varies depending on the identity of the G13 center, exhibiting either donor–acceptor (singlet–singlet) or electron-sharing (triplet–triplet) interactions. According to our computational results, all **G13**=**As-Rea** compounds—except for the B=As analogue—readily undergo 1,3-addition with CH_3I. Energy decomposition analysis combined with natural orbitals for chemical valence (EDA-NOCV), as well as frontier molecular orbital (FMO) theory, indicates that the dominant interaction in these 1,3-addition reactions is the donation from the lone pair on the Ge atom (**G13**=**As-Rea**) into the σ* orbital of the C–I bond in CH_3I. This contrasts with a less favorable interaction involving the filled σ(C–I) orbital donating into the vacant p–π* orbital on G13. The calculated activation barriers are largely governed by the deformation energy of the **G13**=**As-Rea** species, which, in turn, is significantly influenced by the relativistic effects associated with the heavy G13 central atom. Our computational findings reveal a clear correlation between the mass of the G13 atom and the reactivity of the corresponding **G13**=**As-Rea** species in 1,3-addition reactions. As the atomic weight of G13 increases, the relativistic effects become more pronounced, resulting in a contracted ∠G13–As–Ge angle. This geometric feature facilitates superior orbital overlap with CH_3I, thereby lowering the activation barrier and promoting reactivity.

Received 3rd October 2025
Accepted 24th November 2025

DOI: 10.1039/d5ra07521a

rsc.li/rsc-advances

1 Introduction

Molecules featuring a double bond between a group 13 (G13) and a group 15 (G15) element have attracted significant attention due to their fundamental relevance in understanding chemical bonding and molecular structure, as well as their promising potential in various advanced applications.[1–4] Owing to their isoelectronic relationship with classical C=C double bonds, G13=G15 compounds have been explored as candidate materials for semiconductors,[5–9] micro- and nanoelectronic devices,[4,10,11] ultraviolet (UV) photodetectors,[12,13] and hydrogen storage systems.[14] Despite the considerable theoretical efforts devoted to elucidating the nature of G13=G15 multiple bonding,[15–17] the experimental isolation of heavier analogues (G13 = Al–Tl; G15 = P–Bi) remains a substantial challenge.[18–20] This difficulty primarily stems from the intrinsic weakness of the π-bonding interaction, attributed to poor pπ–pπ orbital overlap and enhanced Pauli repulsion between the larger, more diffuse orbitals of heavier main-group elements.[1,3]

Recent breakthroughs in main-group chemistry have enabled the stabilization and isolation of otherwise highly reactive, low-valent species through the use of sterically hindered ligands and donor–acceptor frameworks. These strategies have been instrumental in expanding the structural and electronic diversity of main-group multiple bonds. In particular, a variety of Lewis base (LB)-stabilized heavy imine analogues featuring G13=G15 multiple bonds have now been successfully synthesized and structurally characterized by several pioneering research groups, as illustrated schematically in Fig. 1. These species not only serve as heavier analogues of imines but also offer unique opportunities to explore unconventional bonding and reactivity in main-group systems.[18–20]

A significant milestone was achieved by Power and co-workers,[21,22] who first reported the X-ray crystal structures of B=P and B=As species stabilized by bulky ligands (Fig. 1(I)). Building on this foundation, the research groups of Stephan,[23,24] Bertrand,[23,24] and Braunschweig[25] explored the chemistry of iminoboranes, unveiling a wide range of derivatives functionalized at either the boron or nitrogen centers (Fig. 1(II)–(IV)). These breakthroughs laid the groundwork for the synthesis of

[a]*Department of Applied Chemistry, National Chiayi University, Chiayi 60004, Taiwan. E-mail: midesu@mail.ncyu.edu.tw*
[b]*Department of Medicinal and Applied Chemistry, Kaohsiung Medical University, Kaohsiung 80708, Taiwan*

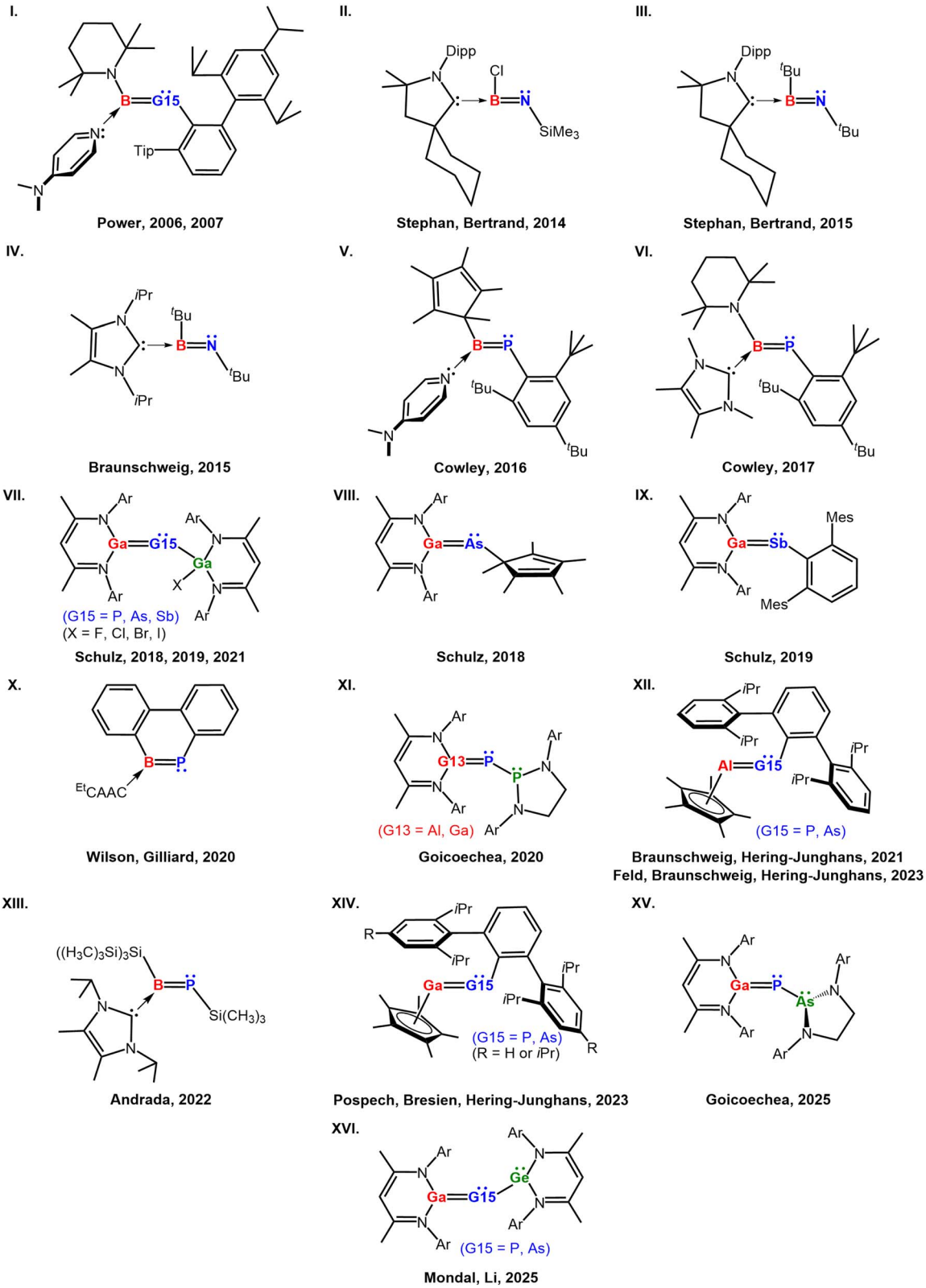

Fig. 1 Selected examples of heavier main-group LB-based imine-type molecules featuring G13=G15 double bonds stabilized by donor ligands. Ar = 2,6-iPr$_2$C$_6$H$_3$. Mes = 2,4,6-tri-*tert*-butylphenyl. Dipp = 2,6-diisopropylphenyl. CAAC = cyclic(alkyl)(amino)carbene.

Lewis base-stabilized B=P compounds by Cowley's group (Fig. 1(V) and (VI))[26,27] and the subsequent development of gallapnictenes by Schulz and co-workers (Fig. 1(VII)–(IX)).[28–35] More recently, Wilson, Gilliard, and collaborators[36] achieved the CAAC-stabilized incorporation of BP into a phenanthryne framework *via* a sequence of decarbonylation, monoatomic

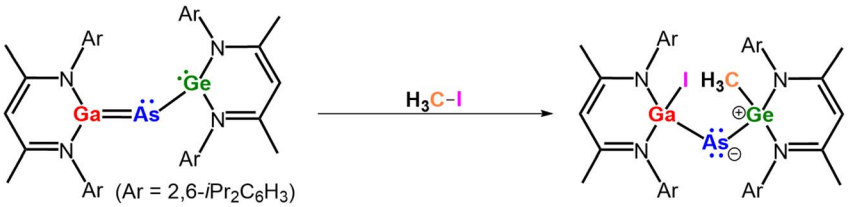

Fig. 2 Synthesis of a zwitterionic 1,3-addition product from the reaction of a germylene-stabilized heavy imine-like (L)Ga═As–Ge(L) species with methyl iodide (where L = CH[C(Me)NAr]$_2$, Ar = 2,6-*i*Pr$_2$C$_6$H$_3$).

phosphide insertion, and ring expansion (Fig. 1(X)). Goicoechea's team[37] subsequently described phosphanyl-substituted gallaphosphenes (Fig. 1(XI)). Parallel efforts by Braunschweig, Hering-Junghans, and their colleagues[38–40] led to the successful synthesis and structural characterization of phosphaalumenes and arsaalumenes, as well as additional gallaphosphenes (Fig. 1(XII) and (XIV)). In a separate advance, Andrada and co-workers[41] reported the synthesis and isolation of an *N*-heterocyclic carbene (NHC)-stabilized phosphaborene bearing a trimethylsilyl (TMS) substituent at the phosphorus center (Fig. 1(XIII)). The most recent contribution by Goicoechea and his team[42] successfully synthesized an arsanylphosphagallene, [H$_2$CN(Dipp)]$_2$AsPGa(NacNac) (NacNac = HC[C(Me)N(Dipp)]$_2$; Dipp = diisopropylphenyl), featuring a mixed G13–G15–G15 bonding motif (Fig. 1(XV)), and investigated its reactivity toward heterocumulenes and ketones. In a separate recent study, Mondal, Li, and their collaborators[43] describes the synthesis of germyl-substituted gallaphosphenes and gallaarsenes (Fig. 1(XV)), thereby broadening the structural diversity of G13–G15–G14 element bonding frameworks. Collectively, these developments have significantly enriched our understanding of low-valent main-group bonding and laid a strong foundation for future reactivity studies and the design of novel functional materials incorporating such unique electronic structures.

As mentioned above, Mondal, Li, and co-workers reported an isolable germylene-stabilized heavy imine-like compound featuring a polarized Ga═As double bond. This compound, (L)Ga═As–Ge(L) (where L = CH[C(Me)NAr]$_2$, Ar = 2,6-*i*Pr$_2$C$_6$H$_3$), exhibited frustrated Lewis pair (FLP) reactivity upon treatment with methyl iodide (Me–I), yielding a zwitterionic 1,3-addition product (Fig. 2).[43] Interestingly, instead of a direct addition across the Ga═As double bond, the reaction proceeds *via* a cooperative interaction between the Ga and Ge centers, unveiling a latent FLP character embedded within the molecular framework.

These findings highlight an unusual reactivity mode and reveal the hidden potential of such heavy imine analogues to function as internal FLPs. Inspired by this advancement, we became interested in exploring the electronic structure and activation barriers associated with their 1,3-addition reactivity. Recent experimental advances have not been matched by equivalent theoretical insight into the bonding nature and mechanisms of germylene-stabilized complexes containing polarized G13═G15 multiple bonds, particularly in mixed G13–G15–G14 architectures.

In this work, we systematically investigate the effect of G13 variation on bonding behavior and activation barriers in germylene-stabilized imine-type molecules possessing G13═As–Ge linkages, as shown in eqn (1). Using density functional theory (DFT) calculations, we offer theoretical insights that not only support experimental observations but also provide a mechanistic rationale for the observed reactivity. These results deepen our understanding of electronic and structural contributions to reactivity and offer guidance for designing new heavy imine-like compounds. We anticipate that these findings will advance the broader field of main group chemistry by illuminating structure–reactivity relationships and stimulating further experimental exploration.

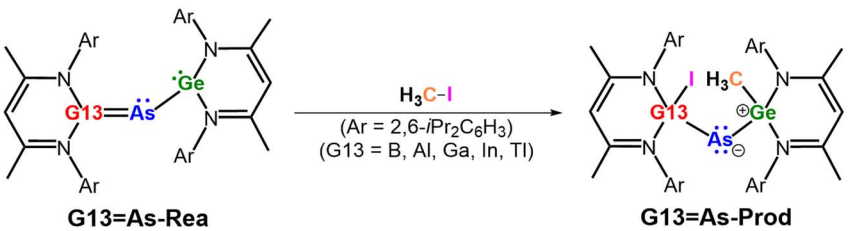

(1)

2 Methodology

In order to achieve a comprehensive understanding of the bonding interactions and reaction mechanisms of heavy-element imine-like systems, a robust computational methodology was adopted. Geometry optimizations and vibrational

frequency analyses were performed at the dispersion-corrected M06-2X[44]-D3 (ref. 45–47)/def2-TZVP[48] level using Gaussian 16 (revision C.01)[49] to ensure the identification of true minima on the potential energy surface. To further elucidate the nature of bonding, energy decomposition analyses (EDAs)[50–55] were carried out using the ADF 2017.112 program.[56] These analyses incorporated relativistic effects *via* the zero-order regular approximation (ZORA)[57,58] and utilized a triple-ζ-quality Slater-type orbital basis set (TZ2P)[59] with polarization functions and a frozen-core approximation. All EDA calculations were performed on geometries optimized at the M06-2X-D3/def2-TZVP level, following the computational protocol denoted as ZORA-M06-2X-D3/TZ2P//M06-2X-D3/def2-TZVP. This hybrid approach, combining accurate structure determination with detailed energetic decomposition, provides reliable insights into the key interactions driving reactivity in systems featuring G13=G15 double bonds, thereby supporting the theoretical foundation of this study.

A quantitative evaluation of the bonding interactions between the heavy imine-like fragment (**G13=As-Rea**) and methyl iodide (CH_3–I) was carried out using the energy decomposition analysis (EDA) method. The total interaction energy (ΔE_{INT}) was dissected into several physically meaningful components as follows:

$$\Delta E_{INT} = \Delta E_{Elstat} + \Delta E_{Pauli} + \Delta E_{Orb} + \Delta E_{Disper} \quad (2)$$

The first term, ΔE_{Elstat}, represents the classical electrostatic interaction between the unperturbed charge distributions of the **G13=As-Rea** fragment and CH_3–I in their transition state geometry (**G13=As-TS**), including the effect of the doubly bonded portion of the heavy imine-like species. The second term, ΔE_{Pauli}, accounts for the Pauli repulsion arising from the antisymmetry requirement of the electronic wavefunction, which prevents same-spin electrons from occupying the same region in space. The third contribution, ΔE_{Orb}, reflects stabilization from orbital interactions, calculated after self-consistent optimization of the Kohn–Sham orbitals. This component can be further analyzed into symmetry-adapted contributions associated with specific irreducible representations. Lastly, ΔE_{Disper} captures the dispersion (van der Waals) interactions between the two fragments.

By employing the natural orbitals for chemical valence (NOCV)[60–63] approach, researchers can visualize the deformation density ($\Delta\rho$), which allows for direct correlation of the ΔE_{Orb} term with specific types of chemical bonding. This visual representation provides valuable insights into charge deformation and redistribution associated with pairwise orbital interactions. Accordingly, the EDA-NOCV method offers not only a quantitative decomposition of orbital interactions but also a qualitative interpretation of the bonding mechanisms involved.

In this study, we aimed to elucidate the key factors controlling the 1,3-addition reactivity of the heavy imine-like fragment **G13=As-Rea** toward methyl iodide. This was achieved by analyzing both the deformation energy (ΔE_{DEF}), required to distort the reactant fragments to the transition state geometry, and the interaction energy (ΔE_{INT}) between the distorted fragments. To further understand the origins of activation barriers in these reactions, we employed the activation strain model (ASM),[64–68] which builds on the distortion/interaction framework initially proposed by Ess and Houk[69–71] and has been widely applied across diverse chemical systems.

3 Results and discussion

3.1 The nature of the G13=As bonding in G13=As-Rea

Before analyzing the 1,3-addition reaction of CH_3–I with doubly bonded G13=As imine-like compounds (eqn (1)), it is essential to first examine the intrinsic bonding characteristics of the G13=As double bond within the **G13=As-Rea** species. The general structure of the **G13=As-Rea** molecule can be described as (LB:→)(L_1)G13=As–L_2, where LB (Lewis base) functions as a two-electron donor, and conventional ligands L_1 and L_2 each contribute one electron to the bonding framework. According to valence bonding model, the most effective approach to describe the bonding features of the G13=As double bond is to conceptually fragment the molecule into two parts: (LB:→)(L_1)G13: and: As–L_2. From a spin-state perspective, two distinct interaction pathways may combine these fragments to generate the singlet ground-state double bond in (LB:→)(L_1)G13=As–L_2.

The first pathway, known as a singlet–singlet interaction or donor–acceptor bonding, involves the combination of two singlet fragments: $[(LB:\rightarrow)(L_1)G13]^1 + [As–L_2]^1 \rightarrow [(LB:\rightarrow)(L_1)G13{=}As–L_2]^1$ (interaction I).

The second pathway, referred to as a triplet–triplet interaction or electron-sharing bonding, arises from the interaction of two triplet fragments: $[(LB:\rightarrow)(L_1)G13]^3 + [As–L_2]^3 \rightarrow [(LB:\rightarrow)(L_1)G13{=}As–L_2]^1$ (interaction II).

These interaction pathways offer valuable insights into the bonding motifs that stabilize such heavy imine-like frameworks and are schematically represented in Fig. 3(a). Particularly, the conclusion derived from the VB theory (Fig. 3(b)) suggests that the ∠G13–G15–L_2 bond angle in a LB-stabilized, doubly bonded imine-like G13=G15 molecule, denoted as (LB:→)(L_1)G13=G15–L_2, is expected to close to 90°. This theoretical prediction is supported by available experimental X-ray crystallographic data,[21–43] showing good agreement with our VB-based structural analysis. The observed angle distortion may also influence the reactivity or stability of these systems, thus offering valuable insight for designing novel FLP-based functional molecules.

The analysis then turns to a detailed examination of the G13=As bonding in **G13=As-Rea** molecules using the energy decomposition analysis (EDA) approach. As established in prior theoretical investigations,[72,73] the key parameter that most accurately reflects the nature of the bonding is the orbital interaction energy (ΔE_{Orb}) which quantifies the extent of orbital interactions between the bonding fragments. In principle, the smaller the change in ΔE_{Orb} upon bond formation, the more accurately the selected fragments represent the true electronic structure of the molecule.[72,73] According to our M06-2X-D3 computational results summarized in Table 1, the absolute values of ΔE_{Orb} for the triplet–triplet electron-sharing

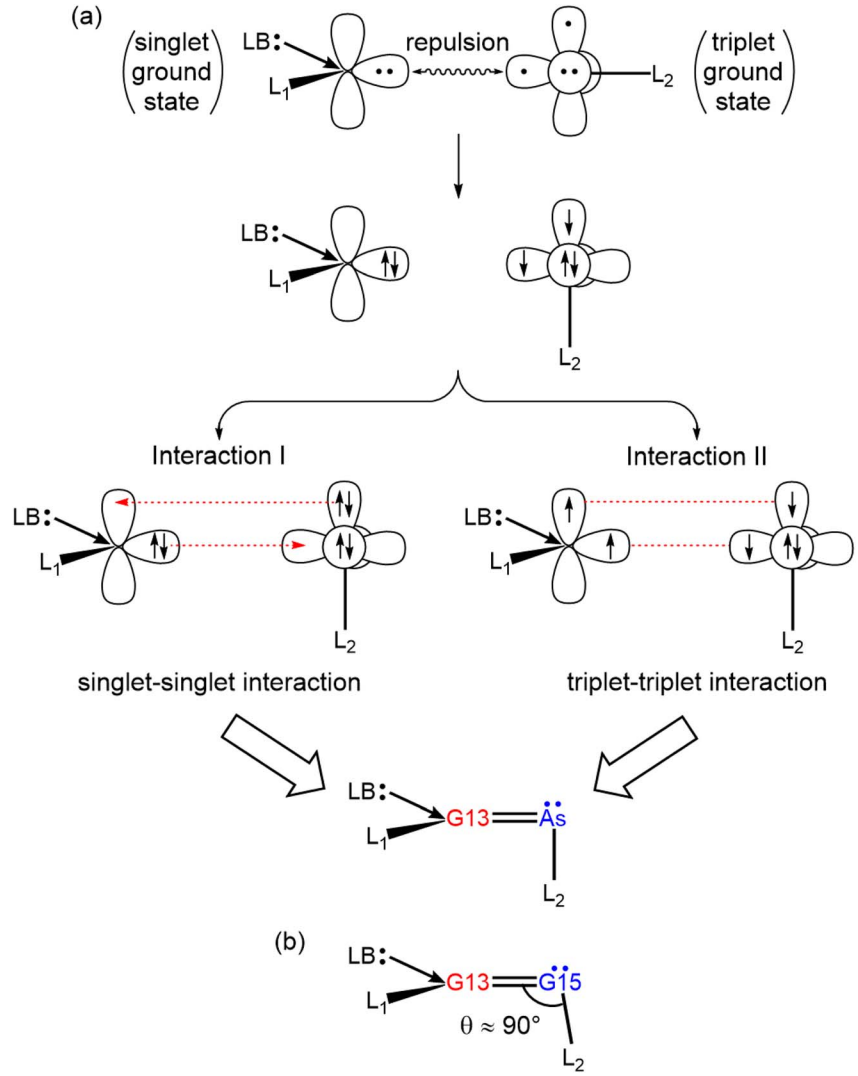

Fig. 3 (a) Valence bonding interactions in the doubly bonded **G13**=**As-Rea** imine-like molecule: a comparison of interaction I (donor–acceptor) and interaction II (electron-sharing). The LB (Lewis base) donates a pair of electrons, while the other conventional ligands, L_1 and L_2, each contribute a single electron to the bonding framework. (b) Based on valence bonding interaction analysis, the ∠G13–G15–L_2 bond angle in the doubly bonded, imine-like molecule (LB:→)(L_1)G13=G15–L_2 is predicted to approach 90°.

interactions in **B**=**As-Rea** and **Al**=**As-Rea** (139.4 and 147.5 kcal mol^{-1}, respectively) are significantly lower than those for the corresponding singlet–singlet donor–acceptor interactions (235.2 and 168.3 kcal mol^{-1}, respectively). These findings suggest that a triplet–triplet electron-sharing mechanism predominantly governs the bonding nature of the G13=As double bond in these imine-like molecules.

In contrast, **Ga**=**As-Rea** can be described by either a classical double bond structure ((L)Ga=As–L_2) or a donor–acceptor formulation of the type (L)Ga ⇆ As–L_2 (where L = CH[C(Me)NAr]$_2$, Ar = 2,6-*i*Pr$_2$C$_6$H$_3$ and L_2 = Ge(L)), as both bonding scenarios exhibit nearly equivalent $|\Delta E_{Orb}|$ values (148.6 kcal mol^{-1} for electron-sharing bonding *vs.* 147.2 kcal mol^{-1} for donor–acceptor bonding). A similar bonding ambiguity was reported previously for a carbene-stabilized Si_2H_2 species.[74]

Meanwhile, for **In**=**As-Rea** and **Tl**=**As-Rea**, the orbital interaction energies favor a donor–acceptor description: the $|\Delta E_{Orb}|$ values for the dative bonds (119.9 and 85.6 kcal mol^{-1}) are noticeably lower than those for the electron-sharing bonds (161.6 and 158.9 kcal mol^{-1}, respectively). These results indicate that the bonding in **In**=**As-Rea** and **Tl**=**As-Rea** is better characterized by a donor–acceptor model, *i.e.*, (L)In ⇆ As–L_2 and (L)Tl ⇆ As–L_2.

Based on the above EDA analysis, it is evident that the G13=As double bond in the LB-based imine-like **G13**=**As-Rea** molecules ((L)G13=As–Ge(L); where L = CH[C(Me)NAr]$_2$ and Ar = 2,6-*i*Pr$_2$C$_6$H$_3$) arises from two principal bonding components: (i) a σ-bond formed by the donation of a lone pair from the sp^2 σ-orbital of the (L)G13: fragment to the vacant σ-orbital of the: As–Ge(L) fragment, and (ii) a dative π-bond originating from a p–π interaction between the lone pair on arsenic and an empty p–π orbital on the G13 center. Due to the significant differences in

Table 1 The nature of the chemical bonding between (L)G13: (where G13 represents a group 13 element and L = CH[C(Me)NAr]$_2$, Ar = 2,6-iPr$_2$C$_6$H$_3$) and : As–L$_2$ (where L$_2$ = Ge(L)) in the **G13=As-Rea** reactant (see eqn (1)) was investigated using Energy Decomposition Analysis (EDA) at the ZORA-M06-2X-D3/TZ2P//M06-2X-D3/def2-TZVP level of theory. The EDA calculations were performed for both singlet (S) and triplet (T) spin states. All computed energy values are reported in kcal mol^{-1}

	B=As-Rea		**Al=As-Rea**		**Ga=As-Rea**		**In=As-Rea**		**Tl=As-Rea**	
Fragments : As–L$_2$ (S)	(L)B: (S) + (T)	(L)B: (T) + : As–L$_2$ (T)	(L)Al: (S) + : As–L$_2$ (S)	(L)Al: (T) + : As–L$_2$ (T)	(L)Ga: (S) + : As–L$_2$ (S)	(L)Ga: (T) + : As–L$_2$ (T)	(L)In: (S) + : As–L$_2$ (S)	(L)In: (T) + : As–L$_2$ (T)	(L)Tl: (S) + : As–L$_2$ (S)	(L)Tl: (T) + : As–L$_2$ (T)
ΔE_{INT} [a]	−134.4	−87.6	−106.4	−120.6	−94.2	−124.5	−79.0	−120.9	−55.3	−95.7
$\Delta E_{\mathrm{Pauli}}$ [b]	391.3	241.0	243.5	169.7	218.3	171.1	170.5	188.4	121.3	201.8
$\Delta E_{\mathrm{Elstat}}$ [b]	−283.8 (54.0%)	−182.4 (55.5%)	−175.3 (50.1%)	−136.6 (47.0%)	−159.2 (50.9%)	−140.7 (47.6%)	−123.7 (49.5%)	−141.6 (46.7%)	−85.1 (48.2%)	−132.7 (44.6%)
ΔE_{Orb} [b]	−235.2 (44.7%)	−139.4 (42.4%)	−168.3 (48.1%)	−147.5 (50.8%)	−147.2 (47.1%)	−148.6 (50.3%)	−119.9 (48.1%)	−161.6 (53.3%)	−85.6 (48.5%)	−158.9 (53.4%)
$\Delta E_{\mathrm{Disper}}$ [b]	−6.7 (1.3%)	−6.7 (2.0%)	−6.2 (1.8%)	−6.2 (2.1%)	−6.2 (2.0%)	−6.2 (2.1%)	−6.0 (2.4%)	−6.0 (1.9%)	−5.9 (3.4%)	−5.9 (2.0%)

[a] $\Delta E_{\mathrm{INT}} = \Delta E_{\mathrm{Elstat}} + \Delta E_{\mathrm{Pauli}} + \Delta E_{\mathrm{Orb}} + \Delta E_{\mathrm{Disper}}$. [b] The values in parentheses offer the percentage contribution to the total attractive interactions ($\Delta E_{\mathrm{Elstat}} + \Delta E_{\mathrm{Orb}}$).

electronegativity and atomic radii between G13 and arsenic, the π-contribution to the G13=As double bond is expected to be relatively weak, especially for the heavier G13 congeners.

The bonding characteristics of G13=As interactions in heavier main-group element frameworks remain a subject of considerable interest due to their deviation from classical double-bond behavior. To gain deeper insight into the electronic nature of these bonds in Lewis base (LB)-stabilized, heavy imine-like **G13=As-Rea** molecules, natural bond orbital (NBO)[75] analysis was conducted. The results, summarized in Table 2, reveal that these bonds are highly polarized and electronically weak. Specifically, the σ-bonds are polarized toward the arsenic atom, with polarization values ranging from 51.17% to 64.84%, while the π-bonds are even more polarized, ranging from 71.79% to 87.33%. The calculated G13–As bond orders fall between 1.313 and 1.664, well below the ideal value of 2.0 expected for a classical double bond. These values indicate only partial double-bond character in the central G13=As linkage of the imine-like **G13=As-Rea** molecules, which incorporate a mixed G13–As–Ge chain. Overall, the NBO analysis confirms that the G13=As double bonds in these LB-stabilized, heavier imine-like systems are relatively weak and electronically fragile, suggesting potential susceptibility to bond cleavage under specific chemical environments.

Furthermore, building upon our understanding of the bonding characteristics in doubly bonded G13=G15 linkages within heavy imine-like molecules, this concept can be extended to related systems featuring formally unsaturated bonding chains such as G13–G15–G13, G13–G15–G14, and G13–G15–G15. For instance, as shown in Fig. 1(VII), Schulz and co-workers[28] have reported a series of imine analogues incorporating a mixed G13–G15–G13 backbone. In contrast, germyl-substituted gallaphosphene and gallaarsene compounds, which feature a G13=G15–G14 bonding motif (Fig. 1(XV)),[43] exhibit structural characteristics analogous to conventional heavy imine-type systems. Likewise, a crystallographically characterized phosphanyl-stabilized gallaphosphene compound containing a G13–G15–G15 bonding chain has been experimentally identified (Fig. 1(XI)).[36] As illustrated in Fig. 4(a)–(c), the VB theory emerges as a powerful and complementary approach for elucidating the electronic structures of these formally unsaturated bonding motifs—namely, G13–G15–G13, G13–G15–G14, and G13–G15–G15. A comprehensive theoretical understanding of these bonding configurations not only enhances our fundamental knowledge of main-group element bonding but also provides valuable guidance for the rational design of novel compounds with potential applications in small-molecule activation and main-group catalysis.[76]

3.2 The 1,3-addition reactions of G13=As-Rea with CH_3I outlined in eqn (1)

To investigate how the identity of the group 13 element influences the activation barrier, we examined the 1,3-addition reactions of germylene-stabilized, doubly bonded imine-like **G13=As-Rea** molecules featuring a G13–As–Ge linkage with methyl iodide (Me–I). As depicted in Fig. 2, the G13 center

Table 2 Natural orbital occupations, polarizations, hybridizations, bond lengths (Å), and Wiberg bond indices (WBI) of the G13–As bond in G13=As-Rea molecules

Molecule	Bond type	Occupancy	Polarization	Hybridization	Bond length (Å)	WBI
B=As-Rea	σ	1.970	B: 48.83% + As: 51.17%	B: $sp^{1.24}d^{0.00}$ As: $sp^{2.79}$ $d^{0.01}$	1.940	1.664
	π	1.864	B: 28.21% + As: 71.79%	B: $sp^{99.99}$ $d^{0.99}$ As: $sp^{1.00}$ $d^{0.00}$		
Al=As-Rea	σ	1.965	Al: 35.16% + As: 64.84%	Al: $sp^{0.31}$ $d^{0.00}$ As: $sp^{4.74}$ $d^{0.04}$	2.265	1.548
	π	1.858	Al: 19.11% + As: 80.89%	Al: $sp^{99.99}$ $d^{15.44}$ As: $sp^{1.00}d^{0.00}$		
Ga=As-Rea	σ	1.967	Ga: 40.74% + As: 59.26%	Ga: $sp^{0.21}$ $d^{0.00}$ As: $sp^{5.99}$ $d^{0.05}$	2.281	1.518
	π	1.864	Ga: 19.24% + As: 80.76%	Ga: $sp^{99.99}$ $d^{16.21}$ As: $sp^{1.00}$ $d^{0.00}$		
In=As-Rea	σ	1.955	In: 44.98% + As: 55.02%	In: $sp^{0.07}$ $d^{0.00}$ As: $sp^{11.73}$ $d^{0.09}$	2.453	1.440
	π	1.855	In: 15.95% + As: 84.05%	In: $sp^{99.99}$ $d^{31.69}$ As: $sp^{1.00}$ $d^{0.00}$		
Tl=As-Rea	σ	1.963	Tl: 38.40% + As: 61.60%	Tl: $sp^{0.03}d^{0.00}$ As: $sp^{22.72}$ $d^{0.18}$	2.493	1.313
	π	1.861	Tl: 12.67% + As: 87.33%	Tl: $sp^{99.99}$ $d^{34.39}$ As: $sp^{99.99}$ $d^{11.32}$		

serves as a Lewis acidic acceptor, whereas the terminal Ge atom functions as a Lewis basic donor. The computed free energy profiles, obtained using the M06-2X-D3/def2-TZVP level of theory, are summarized in Fig. 5. Notably, our computational results indicate that, in the case of **Ga=As-Rea**, the Ga–As bond length, As–Ge bond length, and the ∠Ga–As–Ge bond angle are calculated to be 2.281 Å, 2.495 Å, and 94.3°, respectively—values that are in reasonable agreement with experimental X-ray crystallographic data (2.248 Å, 2.460 Å, and 95.34°, respectively).[43]

On the reactant side, it is noteworthy that all ∠G13–As–Ge bond angles in **G13=As-Rea** molecules fall within the range of 88.9° to 97.6°, which closely approximate to the idealized 90° predicted for doubly bonded imine-like species. These observations are consistent with the VB theory predictions illustrated in Fig. 3(b). Notably, the computed results presented in Fig. 5 reveal a clear decreasing trend in the ∠G13=As–Ge bond angle as the group 13 element changes from B to Tl: **B=As-Rea** (97.6°) > **Al=As-Rea** (95.5°) > **Ga=As-Rea** (94.3°) > **In=As-Rea** (89.8°) > **Tl=As-Rea** (88.9°). This trend correlates with the increasing atomic number of the group 13 element and can be attributed to the relativistic "inert s-pair effect" or "orbital non-hybridization effect".[77–80] In simpler terms, as the G13 element becomes heavier, the s orbital contracts more significantly than the p orbital, leading to a greater size mismatch and reduced s–p orbital overlap. As a result, hybrid orbital formation becomes less efficient, and the heavier G13 center in **G13=As-Rea** compounds tends to favor a more acute ∠G13–As–Ge bond angle.

Despite extensive efforts, no stable van der Waals-type precursor complex could be identified prior to the transition state, implying that the reaction proceeds *via* a concerted mechanism. Our theoretical results, shown in Fig. 5, reveal that the 1,3-addition reactions follow a pathway involving a pseudo-five-membered-ring transition state (**G13=As-TS**), ultimately leading to Me–I bond activation products (**G13=As-Prod**), in which the G13–I and Ge–Me bonds are formed simultaneously. This simultaneous bond formation arises from the cooperative interaction between spatially separated Lewis acidic (G13) and Lewis basic (Ge) centers, thereby unveiling a latent FLP character embedded within the **G13=As-Rea** framework that features a mixed G13=G15–G14 bonding chain.

The reactivity of doubly bonded **G13=As-Rea** molecules toward Me–I was further examined by assessing both the kinetic and thermodynamic feasibility of the 1,3-addition reaction. To properly account for temperature effects and entropy contributions, Gibbs free energies (rather than electronic energies) were used as the basis for comparison. As illustrated in Fig. 5, the computed free activation energies (ΔG_{ACT}, kcal mol^{-1}) for the **G13=As-TS** transition states follow the decreasing trend: **B=As-TS** (31.2) > **Al=As-TS** (23.6) > **Ga=As-TS** (19.4) > **In=As-TS** (16.3) > **Tl=As-TS** (11.4). This trend clearly suggests that the activation barrier decreases with increasing atomic number of the G13 center in the **G13=As-Rea** framework. Similarly, the corresponding reaction free energies (ΔG_{RXN}, kcal mol^{-1}) are all exergonic and follow a similar descending order: **B=As-Prod** (−23.6) > **Al=As-Prod** (−51.3) > **Ga=As-Prod** (−58.8) > **In=As-Prod** (−63.2) > **Tl=As-Prod** (−64.8). These results imply that both the kinetic and thermodynamic favorability of the 1,3-addition reaction with Me–I increases as the G13 center becomes heavier. Therefore, our M06-2X-D3/def2-TZVP computational data strongly suggest that, with the exception of the **B=As-Rea** species (which shows a prohibitively high barrier), all other heavier imine-like **G13=As-Rea** compounds are predicted to undergo spontaneous 1,3-addition with methyl iodide at ambient conditions. Taken together, these results

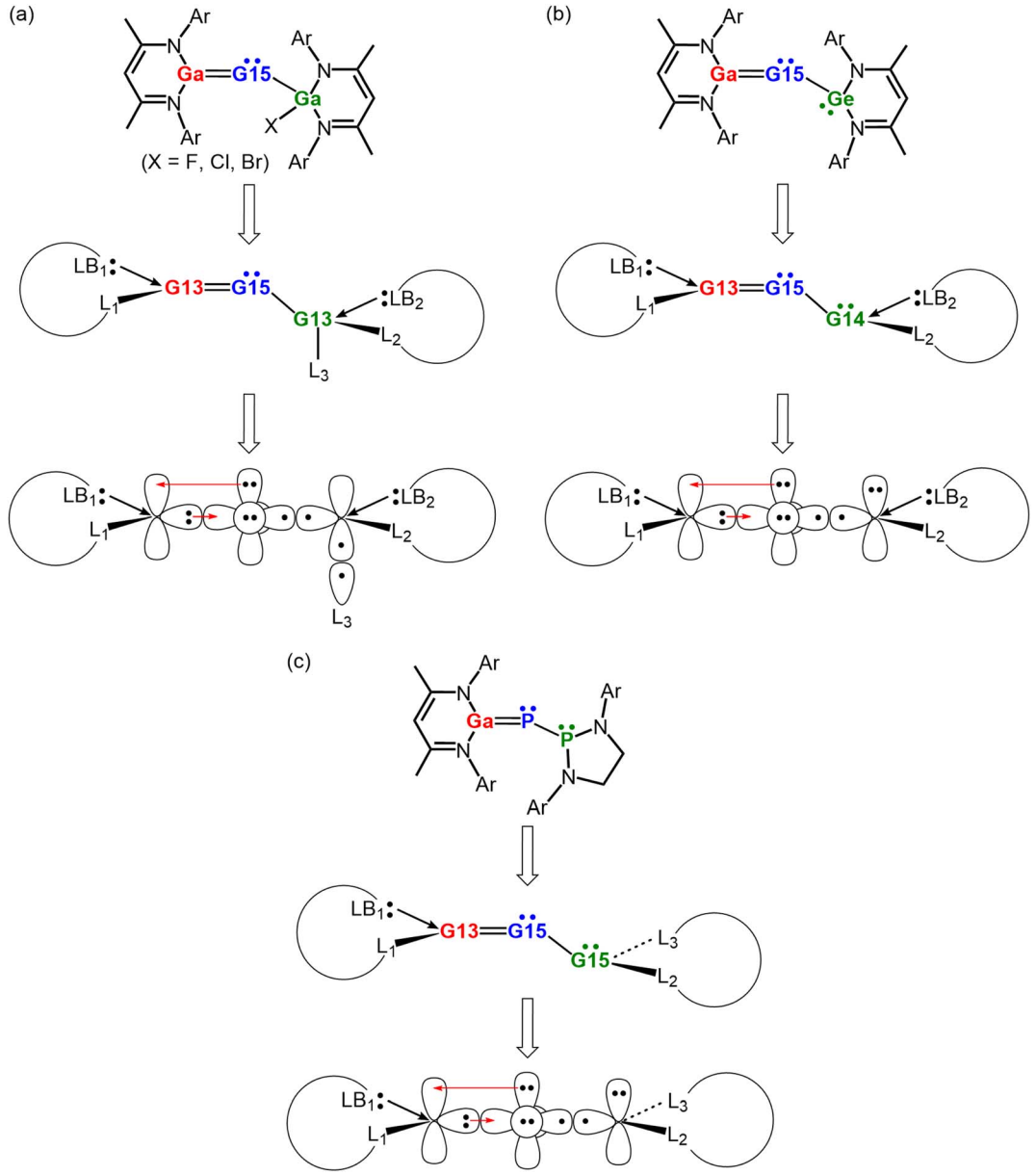

Fig. 4 Valence bonding interactions in strongly π-conjugated G13═G15 imine-like molecules, featuring formally unsaturated bonding chains of (a) G13═G15–G13, (b) G13═G15–G14, and (c) G13═G15–G15. Experimental examples corresponding to these bonding motifs are illustrated in Fig. 1(VI), (XII) and (IX), respectively. LB = Lewis base, which is a two-electron donor. L_1, L_2, and L_3 are one-electron contributors.

highlight the influence of periodic trends on main-group reactivity and support the utility of heavy group 13 elements in FLP-like bond activation processes. Notably, the above theoretical prediction is in good agreement with the experimental observations reported by Mondal, Li, and co-workers on the **Ge═As-Rea** system.[43] These theoretical findings not only provide guidance for experimental chemists in designing further studies to validate them, but also expand the conceptual framework of FLP-type behavior in heavier p-block systems, particularly with respect to the reactivity of multiple bonds in main-group compounds.[36,81] Such insights substantially deepen our understanding of main-group reactivity and provide a theoretical foundation for the rational design of novel catalytic platforms based on cooperative activation mechanisms.

3.3 FMO analysis

To gain a deeper understanding of the origin of the reaction barriers in the 1,3-addition reactions between germylene-stabilized imine-like **G13═As-Rea** molecules and CH_3I, we performed a detailed electronic structure analysis based on frontier molecular orbital (FMO)[82] theory. As shown in Fig. 6, the molecular orbital diagrams display both the spatial distributions and energy levels (in eV) of the relevant orbitals. Notably, the highest occupied molecular orbital (HOMO) of **G13═As-Rea** is mainly localized on the Lewis basic germanium center,

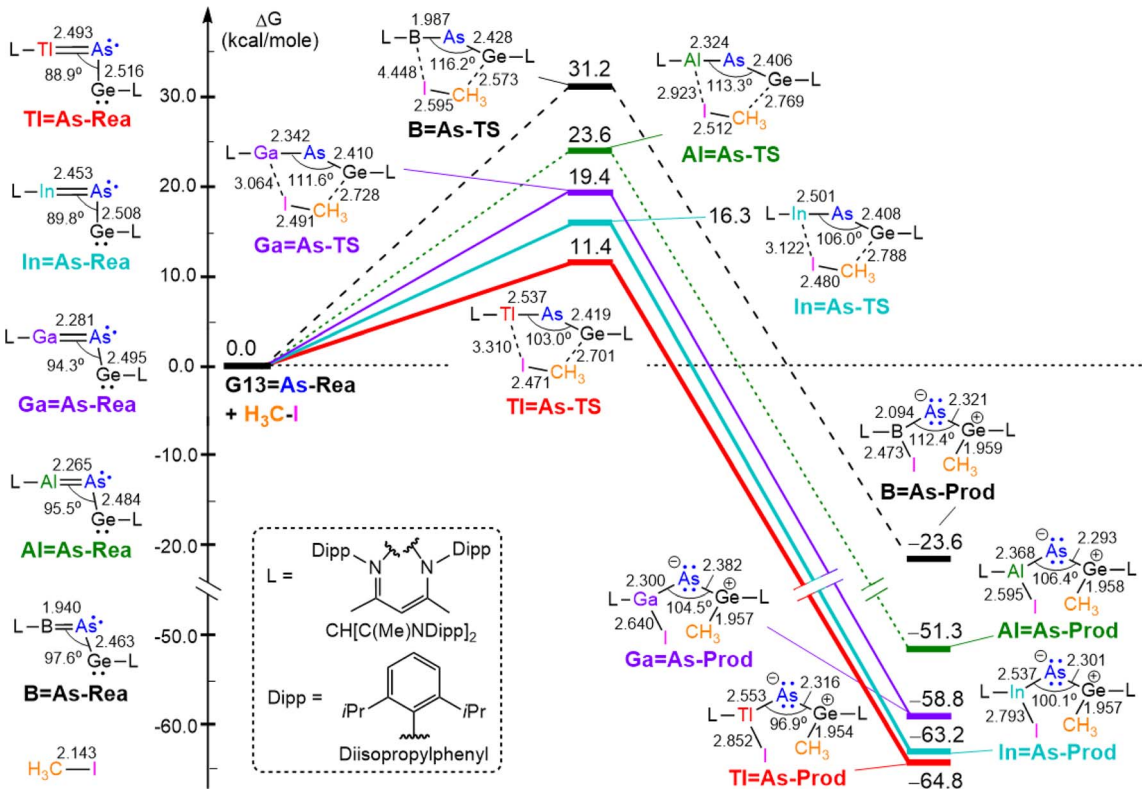

Fig. 5 Free energy profiles for the 1,3-addition of CH_3–I to doubly bonded **G13=As-Rea** imine-like compounds *via* the transition state (**G13=As-TS**) leading to the final product (**G13=As-Prod**): relative free energies (kcal mol^{-1}), bond lengths (Å), and bond angles (°) calculated at the M06-2X-D3/def2-TZVP level.

whereas the p–π*(G13=As) orbital is predominantly distributed over the Lewis acidic G13 element. Based on the orbital energy data summarized in Fig. 6 and Table 3 reports the energy differences between (i) the LUMO of CH_3I, identified as a σ*(C–I) orbital, and the HOMO of **G13=As-Rea**, and (ii) the p–π*(G13=As) orbital of **G13=As-Rea** and the HOMO of CH_3I, which is a lone pair orbital primarily localized on the iodine atom. For all systems examined, the energy gaps associated with the former interaction (4.950–5.605 kcal mol^{-1}) are significantly smaller than those of the latter (8.617–8.937 kcal mol^{-1}). Based on the FMO theory, a smaller energy gap typically corresponds to a stronger orbital interaction, whereas a larger gap suggests a weaker interaction. Accordingly, the FMO results presented in Table 3 strongly indicate that the dominant orbital interaction in the 1,3-addition reaction most likely occurs between the HOMO of the germylene-supported imine-like **G13=As-Rea** species and the LUMO of CH_3I. This interaction pattern will be further validated through the subsequent EDA-NOCV analysis, which provides detailed insight into the nature and strength of the contributing orbital components.

3.4 EDA-NOCV analysis

Before performing the EDA-NOCV analysis of the 1,3-addition reactions between the germylene-supported imine-like **G13=As-Rea** molecules and CH_3I, it is crucial to first investigate the nature of the bonding interactions that arise during their association. This preliminary examination offers valuable insight into the fundamental origin of the observed activation barriers. Both the **G13=As-Rea** species and CH_3I are characterized as singlet ground-state molecules. Consequently, their interaction can give rise to two distinct bonding scenarios: a singlet–singlet interaction, often referred to as a donor–acceptor interaction, and a triplet–triplet interaction, commonly described as an electron-sharing interaction.

As schematically depicted in Fig. 7, the chemical bonding between the **G13=As-Rea** species—which features a mixed G13–G15–G14 chain—and CH_3I in the singlet–singlet electronic configuration can be rationalized by two principal orbital interactions. First, two electrons from the HOMO of **G13=As-Rea**, corresponding to a lone pair localized on the Ge atom, are donated into the LUMO of CH_3I, which is the σ* antibonding orbital of the **H_3C–I** bond. Second, a stabilizing back-donation takes place from the HOMO of CH_3I (the lone pair orbital of the I atom) into the unoccupied orbital of **G13=As-Rea**, which corresponds to a vacant p–π* orbital located at the G13 site. As a consequence, this dual orbital interaction can be described as follows: HOMO of **G13=As-Rea** (Ge lone pair) → LUMO of CH_3I (**H_3C–I** σ* orbital), and HOMO of CH_3I (I lone pair) → the unoccupied orbital of **G13=As-Rea** (empty p–π* orbital of G13). This bonding scenario is consistent with a donor–acceptor model in which the interaction between these two singlet species forms the transition state [**G13=As–TS**]^1 through the combination of [**G13=As-Rea**]^1 and [**H_3C–I**]^1. Accordingly, two dative bonds—Ge → C and Ga ← I—are proposed to form

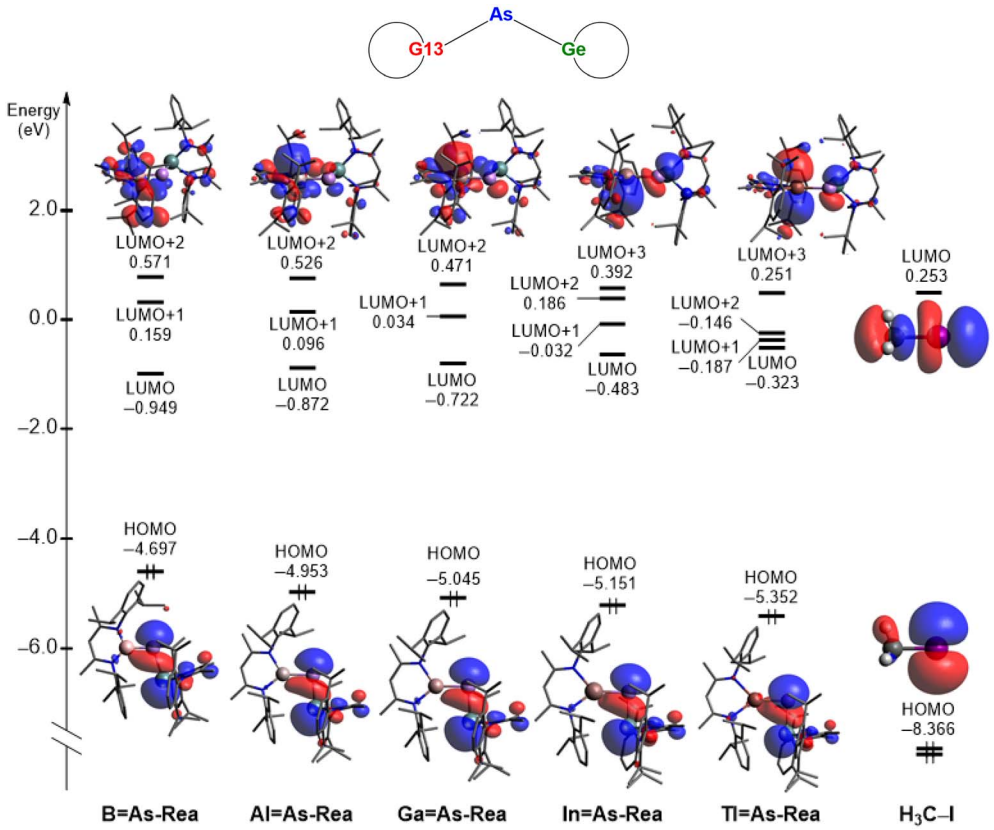

Fig. 6 Selected frontier molecular orbitals (HOMO and LUMO) and their energies (in eV) for imine-like **G13**=**As-Rea** molecules and methyl iodide.

during the 1,3-addition reaction of the imine-like **G13**=**As-Rea** molecule with CH_3I.

In the triplet–triplet electronic interaction model, both the imine-like **G13**=**As-Rea** reactant and CH_3I are considered in their respective triplet states. As shown in Fig. 8, their interaction leads to the formation of a transition state, **G13**=**As-TS**, in an overall singlet electronic configuration. This process can be denoted as $[\mathbf{G13{=}As\text{-}Rea}]^3 + [\mathbf{H_3C{-}I}]^3 \rightarrow [\mathbf{G13{=}As\text{-}TS}]^1$. Within this electron-sharing framework, it is inferred that two covalent bonds—Ge–C and Ga–I—are formed as a result of direct spin-paired electron exchange between the two fragments.

It is noteworthy that the donor–acceptor model, in which a lone pair on Ge is donated into the σ* orbital of $\mathbf{H_3C{-}I}$, closely resembles Fischer-type[83] carbene bonding (Scheme 1(a)). Conversely, the triplet–triplet electron-sharing interaction, characterized by covalent bond formation *via* spin-paired electrons, is reminiscent of Schrock-type[84] bonding (Scheme 1(b)). These electronic representations parallel highlight the potential for main-group species to emulate bonding behaviors traditionally associated with d-block transition metals.[85]

To gain deeper insight into the bonding characteristics between **G13**=**As-Rea** and CH_3I, we performed EDA-NOCV calculations on the corresponding transition structure, **G13**=**As-TS**. These analyses were carried out using two distinct fragmentation schemes: one based on the singlet–singlet (donor–acceptor) bonding model and the other on the triplet–triplet (electron-sharing) bonding model, as depicted in Fig. 7 and 8, respectively. The numerical outcomes of these

Table 3 Energy difference (in eV) between the frontier molecular orbitals of imine-like **G13**=**As-Rea** and methyl iodide according to eqn (1), calculated at the M06-2X-D3/def2-TZVP level

System	Energy difference CH_3I (LUMO) – G13 = As-Rea (HOMO)	Energy difference G13 = As-Rea (p–π*) – CH_3I (HOMO)
B=**As-Rea** + CH_3I	4.950	8.937[a]
Al=**As-Rea** + CH_3I	5.206	8.892[a]
Ga=**As-Rea** + CH_3I	5.398	8.837[a]
In=**As-Rea** + CH_3I	5.404	8.758[b]
Tl=**As-Rea** + CH_3I	5.605	8.617[b]

[a] According to Fig. 6, this value is obtained from bent **G13**=**As-Rea** (LUMO+2) – CH_3I (HOMO). [b] According to Fig. 6, this value is obtained from bent **G13**=**As-Rea** (LUMO+3) – CH_3I (HOMO).

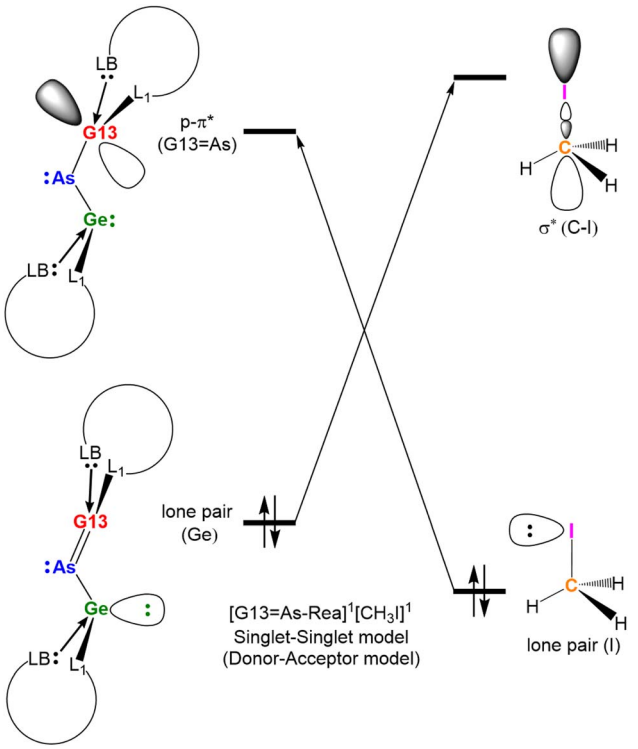

Fig. 7 Singlet–singlet (donor–acceptor) bonding model for the 1,3-addition reaction between the imine-like **G13**=**As-Rea** molecule and CH_3I. The **G13**=**As-Rea** species is represented as (LB)(L_1)G13=As–Ge(LB)(L_1), where G13 denotes a group 13 element and (LB)(L_1) refers to the CH[C(Me)NAr]$_2$ (Ar = 2,6-*i*Pr$_2$C$_6$H$_3$) ligand framework.

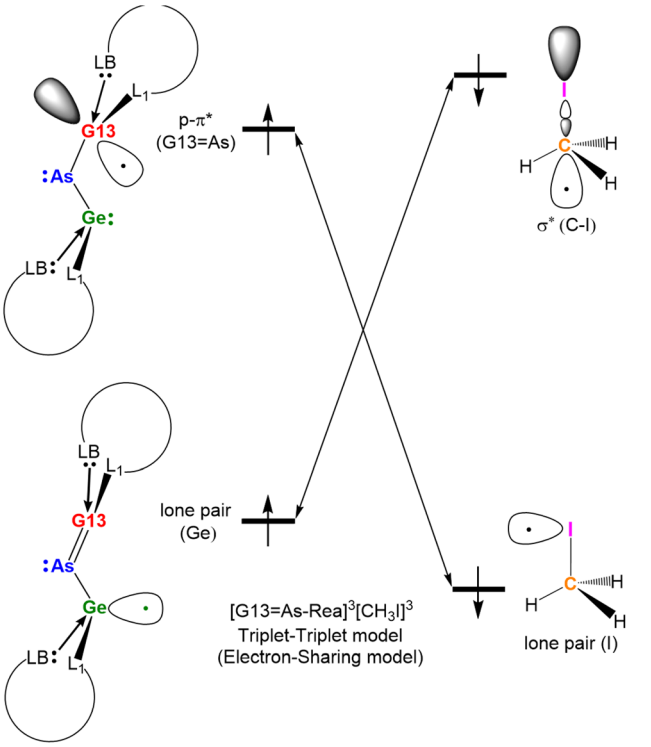

Fig. 8 Triplet–triplet (electron-sharing) bonding model for the 1,3-addition reaction between the imine-like **G13**=**As-Rea** molecule and CH_3I. The **G13**=**As-Rea** species is represented as (LB)(L_1)G13=As–Ge(LB)(L_1), where G13 denotes a group 13 element and (LB)(L_1) refers to the CH[C(Me)NAr]$_2$ (Ar = 2,6-*i*Pr$_2$C$_6$H$_3$) ligand framework.

computations are summarized in Table 4. Importantly, the most suitable fragmentation scheme is generally identified by the lowest orbital interaction energy (ΔE_{Orb}),[61,62] which reflects the minimal orbital distortion required to form the electronic structure of the full complex. Thus, a smaller ΔE_{Orb} value corresponds to a more accurate and energetically favorable bonding representation.[68,69] As shown in Table 4, the singlet–singlet model yields a substantially lower absolute value of ΔE_{Orb} ($|\Delta E_{Orb}|$ = 35.7–44.4 kcal mol^{-1}) compared to that of the triplet–triplet model ($|\Delta E_{Orb}|$ = 134.9–220.3 kcal mol^{-1}). This result indicates that the bonding interaction in **G13**=**As-TS** is best described as two dative bonds—namely, Ge → C and G13 ← I. Consequently, we adopted the singlet–singlet (donor–acceptor) framework for all subsequent analyses to explore the electronic structure of the bonding interaction between **G13**=**As-Rea** and CH_3I.

As shown in Table 4, the total orbital interaction energy (ΔE_{Orb}) is decomposed into three components: two dominant pairwise orbital contributions, $\Delta E_{Orb(1)}$ and $\Delta E_{Orb(2)}$, and a residual term, ΔE_{Rest}. Notably, the sum of $\Delta E_{Orb(1)}$ and $\Delta E_{Orb(2)}$ accounts for at least 71.3% of the total ΔE_{Orb}, and these two primary interactions are illustrated graphically in Fig. 9. As depicted in Fig. 9, the most significant deformation density, $\Delta\rho_{(1)}$, corresponds to $\Delta E_{Orb(1)}$, which primarily originates from charge transfer from the lone pair orbital on Ge (in **G13**=**As-Rea**) into the vacant σ* orbital of the C–I bond in CH_3I. This interaction reflects a classical donor–acceptor process involving the HOMO of **G13**=**As-Rea** and the LUMO of CH_3I, resulting in the formation of a Ge → C dative bond. In contrast, $\Delta E_{Orb(2)}$ arises from electron donation from the filled σ orbital of the C–I bond in CH_3I to the vacant p–π* orbital on G13 (in **G13**=**As-Rea**). This represents a reverse donor–acceptor interaction involving the HOMO of CH_3I and the LUMO of **G13**=**As-Rea**, leading to the formation of a G13 ← I dative bond. These NOCV results agree well with the FMO analysis presented in Fig. 6 and Table 3, jointly supporting the donor–acceptor bonding character in the formation of **G13**=**As-TS**.

3.5 ASM analysis

To gain deeper insight into the origin of the activation barriers in the 1,3-addition reactions and to identify the key factor contributing to their magnitudes, the ASM analysis was carried out to examine the evolution of energy components associated with the formation of the **G13**=**As-TS** transition states. These

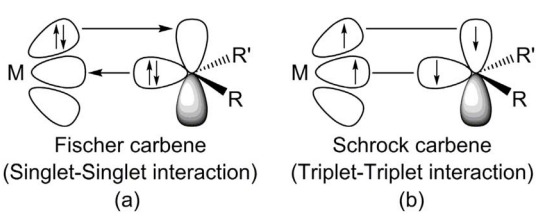

Scheme 1 Schematic representation of the bonding interactions in (a) Fischer-type and (b) Schrock-type metal carbenes.

Table 4 Energy decomposition analysis results of **G13=As-TS** using both singlet–singlet and triplet–triplet models at the ZORA-M06-2X-D3/TZ2P//M06-2X-D3/def2-TZVP level[a]

Fragments	**B=As-TS**		**Al=As-TS**		**Ga=As-TS**		**In=As-TS**		**Tl=As-TS**	
	B=As-Rea (S) + H_3C–**I** (S)	**B=As-Rea** (T) + H_3C–**I** (T)	**Al=As-Rea** (S) + H_3C–**I** (S)	**Al=As-Rea** (T) + H_3C–**I** (T)	**Ga=As-Rea** (S) + H_3C–**I** (S)	**Ga=As-Rea** (T) + H_3C–**I** (T)	**In=As-Rea** (S) + H_3C–**I** (S)	**In=As-Rea** (T) + H_3C–**I** (T)	**Tl=As-Rea** (S) + H_3C–**I** (S)	**Tl=As-Rea** (T) + H_3C–**I** (T)
ΔE_{INT} [b]	−22.5	−195.7	−22.0	−159.8	−21.2	−100.7	−21.0	−123.5	−19.8	−124.5
ΔE_{Pauli}	60.2	55.8	83.4	50.4	72.1	71.4	70.8	123.0	63.3	84.2
ΔE_{Elstat} [c]	−42.4 (51.3%)	−29.2 (11.6%)	−59.1 (56.0%)	−19.4 (9.2%)	−51.8 (55.5%)	−35.3 (20.5%)	−52.1 (56.8%)	−82.8(33.6%)	−45.5 (54.8%)	−56.5(27.1%)
ΔE_{Orb} [c]	−38.4 (46.4%)	−220.3 (87.6%)	−44.4 (42.1%)	−188.8 (89.8%)	−39.6 (42.4%)	−134.9(78.4%)	−37.8 (41.1%)	−161.7(65.6%)	−35.7 (42.9%)	−150.2(72.0%)
$\Delta E_{Orb(1)}$ [d]	−23.4 (61.1%)	−137.8 (62.6%)	−18.7 (42.2%)	−168.9(89.5%)	−16.7 (42.3%)	−107.8(79.9%)	−16.7 (44.1%)	−132.4(81.9%)	−17.1 (47.8%)	−125.3(83.4%)
$\Delta E_{Orb\ (2)}$ [d]	−11.1 (29.0%)	−41.5 (18.8%)	−12.9 (29.1%)	−11.8(6.3%)	−13.1 (33.1%)	−17.9(13.3%)	−11.9 (31.4%)	−17.0(10.5%)	−10.5 (29.4%)	−17.4(11.6%)
ΔE_{Rest} [d]	−3.8 (9.9%)	−41.0 (18.6%)	−12.7 (28.7%)	−8.1(4.2%)	−9.7 (24.6%)	−9.2(6.8%)	−9.2 (24.5%)	−12.3(7.6%)	−8.1 (22.8%)	−7.5(5.0%)
ΔE_{Disper} [c]	−1.9 (2.3%)	−1.9 (0.8%)	−2.0 (1.9%)	−2.0 (0.9%)	−2.0 (2.1%)	−2.0(1.1%)	−1.9 (2.1%)	−1.9(0.8%)	−1.9 (2.3%)	−1.9(0.9%)

[a] Energy values are presented in kcal mol^{-1} for all measurements. [b] $\Delta E_{INT} = \Delta E_{Elstat} + \Delta E_{Pauli} + \Delta E_{Orb} + \Delta E_{Disper}$. [c] The values in parentheses represent the percentage contribution of (ΔE_{Elstat} + ΔE_{Orb} + ΔE_{Disper}) to the total attractive interactions. [d] The values enclosed in parentheses indicate the percentage of the total orbital interactions (ΔE_{Orb}) that they contribute.

calculations were performed at the ZORA-M06-2X-D3/TZ2P//M06-2X-D3/def2-TZVP level of theory, with the results summarized in Table 5. In general, the activation energy (ΔE_{ACT}) can be decomposed into two principal components: the deformation energy of the reactants ($\Delta E_{DEF} = \Delta E_{DEF,G13=As\text{-}Rea} + \Delta E_{DEF,CH_3I}$) and the interaction energy between the deformed fragments (ΔE_{INT}). Fig. 10 displays the reaction energy profiles for each component across the **G13=As-TS** systems.

Our ASM results, as depicted in Fig. 10, reveal that the primary contributor to the variation in activation barriers among the **G13=As-TS** systems arises from differences in the deformation energy of methyl iodide ($\Delta E_{DEF,CH_3I}$). Specifically, the elevated activation energies in certain systems can be attributed to the significant geometric distortion required by the CH_3–I fragment during the formation of the transition state. For instance, the $\Delta E_{DEF,CH_3I}$ value associated with the **B=As-TS** system is the highest among all **G13=As-TS** cases, correlating with the highest overall activation energy observed. This behavior can be rationalized as follows: during the 1,3-addition reaction between CH_3I and **G13=As-Rea**, which features a mixed G13–As–Ge backbone, the G13-based Lewis acid and the Ge-based Lewis base must simultaneously approach the CH_3–I molecule to facilitate bond formation. As shown in Fig. 5, the ∠G13–As–Ge angle becomes increasingly acute with heavier group 13 elements, primarily due to relativistic effects.[77–80] To attain optimal orbital overlap between the imine-like **G13=As-Rea** species and CH_3–I, both fragments must undergo conformational adjustments. However, the **G13=As-Rea** moiety, being relatively bulky, possesses limited geometric flexibility. In contrast, CH_3–I, owing to its compact size, is more easily deformed. As a result, the deformation energy of CH_3–I varies significantly with the ∠G13–As–Ge angle. As the atomic number of G13 increases, the ∠G13–As–Ge angle decreases, reducing the distance between the G13 and Ge centers. This structural contraction enhances the orbital overlap with CH_3–I, facilitates C–I bond cleavage, and promotes product formation (**G13=As-Prod**). In the case of **B=As-Rea**, however, the bending of the ∠B–As–Ge angle required in the transition state (**B=As-TS**) is particularly pronounced. This leads to substantial geometric distortion of the CH_3–I fragment, resulting in a significantly higher $\Delta E_{DEF,CH_3I}$ compared to those of the heavier G13 analogues, as clearly illustrated in Fig. 10.

Further support for the above conclusion is provided by the analysis of geometric changes shown in Fig. 5. In particular, the percentage decrease in the ∠G13–As–Ge bond angle upon transition state formation follows the trend: 19.1% (**B=As-TS**) > 18.6% (**Al=As-TS**) > 18.3% (**Ga=As-TS**) > 18.0% (**In=As-TS**) > 15.9% (**Tl=As-TS**). This sequence closely parallels the corresponding trend observed in activation energies (Fig. 5). Additionally, according to the geometrical data in Fig. 5, the extent of H_3C–**I** bond elongation at the **G13=As-TS** point—relative to its original length of 2.143 Å—follows the order: 21.1% (**B=As-TS**) > 17.2% (**Al=As-TS**) > 16.2% (**Ga=As-TS**) > 15.7% (**In=As-TS**) > 15.3% (**Tl=As-TS**). These observed geometric distortions are in good agreement with the computed activation barriers, indicating that smaller G13 elements (*e.g.*, B or Al) experience more pronounced structural deformation, which in turn contributes

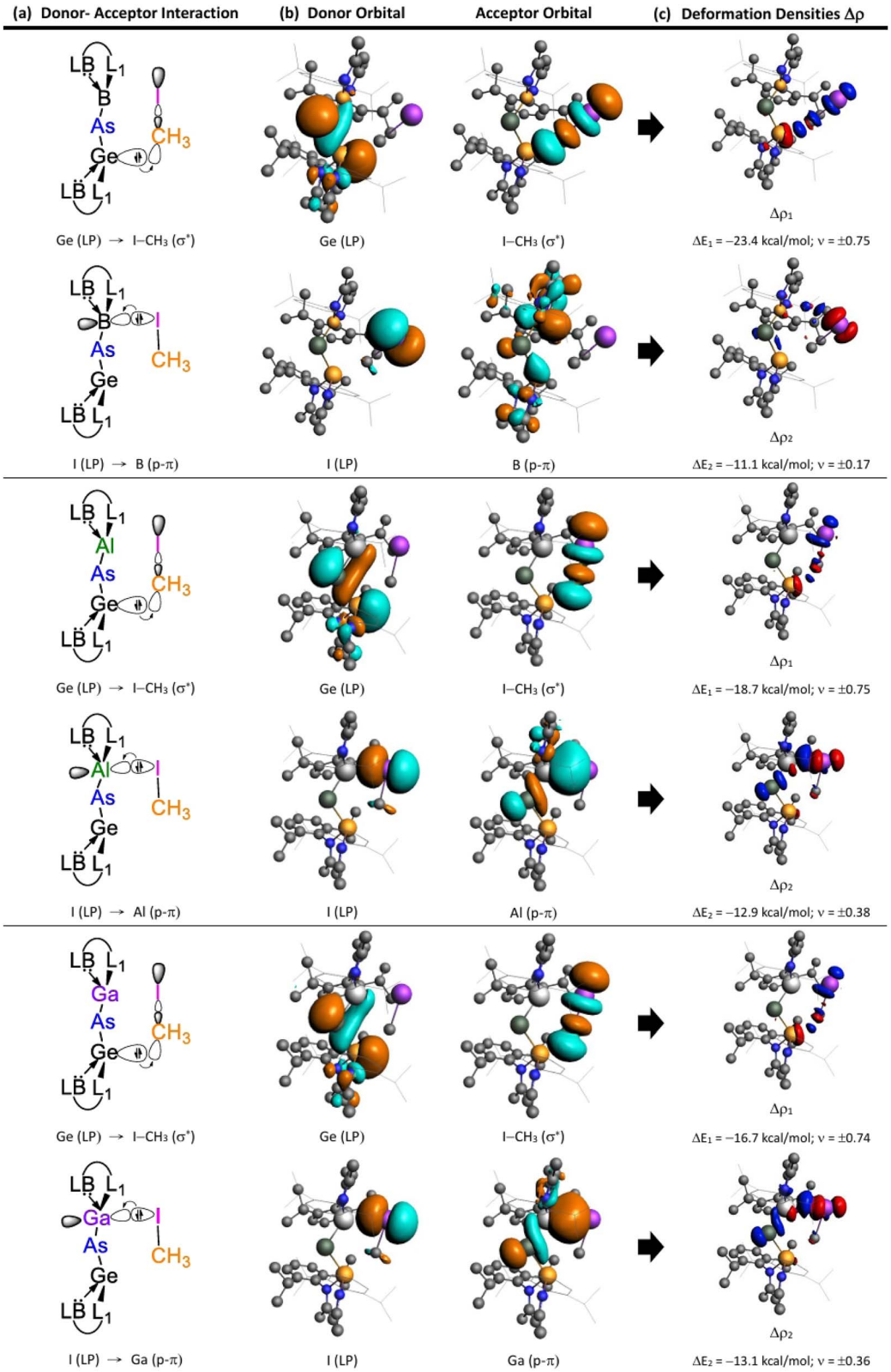

Fig. 9 EDA-NOCV analysis of **G13=As-TS**: (a) schematic illustration of key orbital interactions between the fragments **G13=As-Rea** and CH_3I. (b) Visualization of the most significant orbital overlap between the occupied orbitals of one fragment and the unoccupied orbitals of the other. (c) Deformation density plots ($\Delta\rho$) corresponding to pairwise orbital interactions between the closed-shell fragments, along with their associated orbital interaction energies, $\Delta E_{Orb(1)}$ and $\Delta E_{Orb(2)}$ (in kcal mol^{-1}). Red → blue arrows indicate the direction of charge flow in each deformation density map.

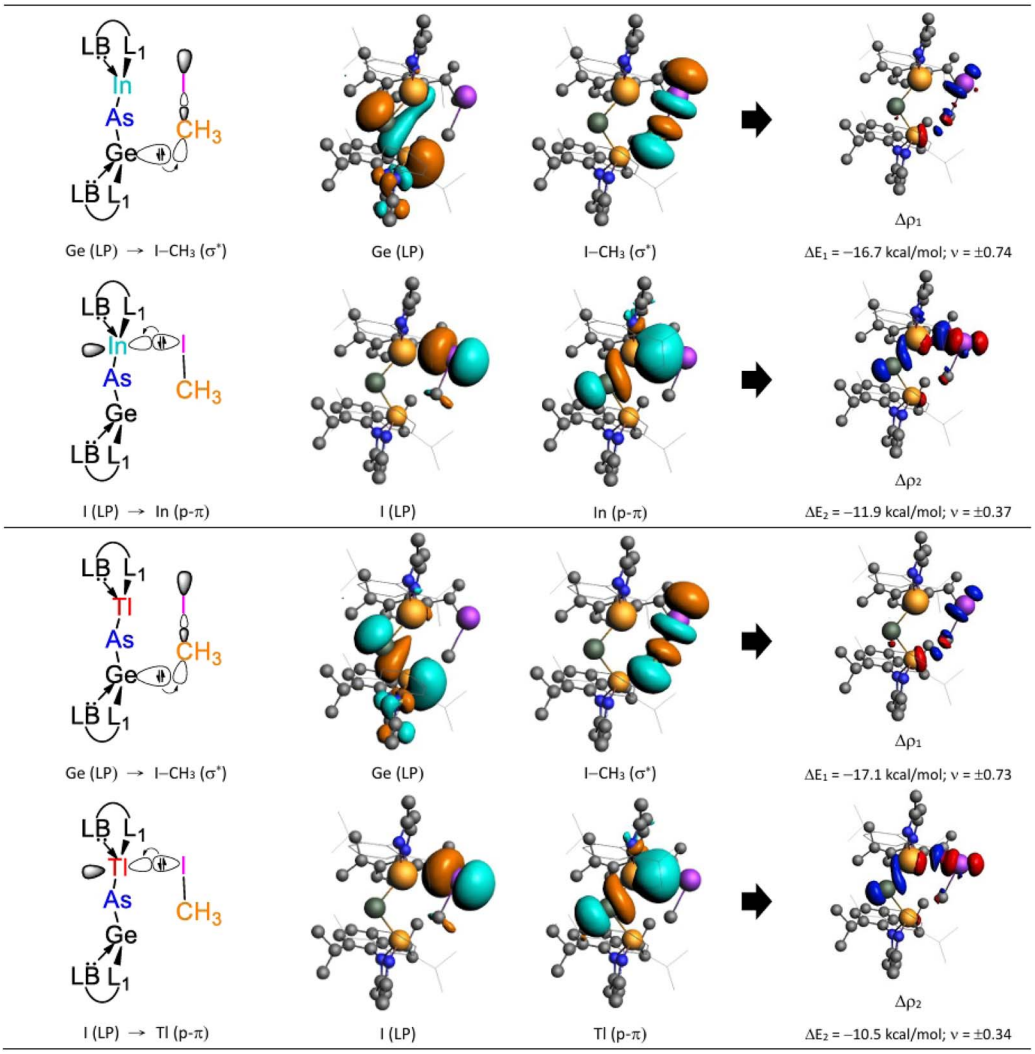

Fig. 9 (*Contd.*)

to higher activation energies. This correlation is consistent with Hammond's postulate,[86] which posits that transition states more structurally similar to reactants tend to be associated with lower activation barriers, while those more product-like correspond to higher energy profiles in less exergonic reactions. Altogether, these results highlight the critical role of geometric deformation in modulating the reactivity of main-group element-based systems.

To better understand the origin of the reactivity differences between various G13=As-based imine analogues in 1,3-addition reactions, we carried out an ASM analysis focusing on two representative transition structures, **C=As-TS** (black) and **Tl=As-TS** (red). As depicted in Fig. 11, the deformation energy associated with the **G13=As-Rea** fragment plays a dominant role in determining the reaction barrier. While the strain and interaction energy contributions from the **G13=As-Rea** framework ($\Delta E_{\mathrm{DEF,G13=As\text{-}Rea}}$) and the total interaction energy (ΔE_{INT}) remain nearly constant between the two systems, the deformation energy of CH_3I ($\Delta E_{\mathrm{DEF,CH_3I}}$) differs significantly. Notably, as shown in Fig. 11, the CH_3I moiety in the **Tl=As-TS** system exhibits substantially lower deformation energy along the entire reaction coordinate, which correlates with its reduced activation barrier and enhanced reactivity. These results not only rationalize the periodic trend observed in Fig. 5 but also demonstrate the power of ASM in deconstructing activation energies into chemically intuitive components. Such findings

Table 5 ASM analysis of **G13=As-Rea** and methyl iodide in **G13=As-TS** at the ZORA-M06-2X-D3/TZ2P//M06-2X-D3/def2-TZVP level. The unit of energy is kcal mol^{-1}

Entry	B=As-TS	Al=As-TS	Ga=As-TS	In=As-TS	Tl=As-TS
$\Delta E_{\mathrm{ACT}}{}^{a}$	20.6	14.4	11.0	8.0	5.8
$\Delta E_{\mathrm{DEF,G13=As\text{-}Rea}}{}^{b}$	21.2	20.0	18.9	18.1	16.6
$\Delta E_{\mathrm{DEF,CH3I}}{}^{b}$	21.9	16.4	13.3	10.9	9.0
ΔE_{INT}	−22.5	−22.0	−21.2	−21.0	−19.8

^{a} $\Delta E_{\mathrm{ACT}} = \Delta E_{\mathrm{DEF,G13=As\text{-}Rea}} + \Delta E_{\mathrm{DEF,CH3I}} + \Delta E_{\mathrm{INT}}$. ^{b} $\Delta E_{\mathrm{DEF}} = \Delta E_{\mathrm{DEF,G13=As\text{-}Rea}} + \Delta E_{\mathrm{DEF,CH3I}}$.

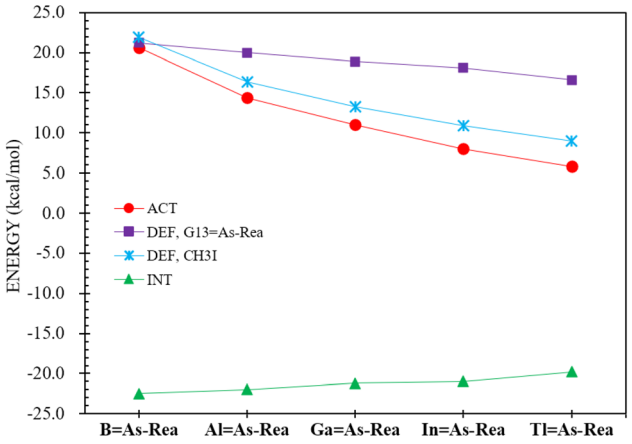

Fig. 10 Energy decompositions of ΔE_{ACT} of **G13=As-TS** for 1,3-addition reactions of **G13=As-Rea** with methyl iodide at the ZORA-M06-2X-D3/TZ2P//M06-2X-D3/def2-TZVP level. Also, see Table 5.

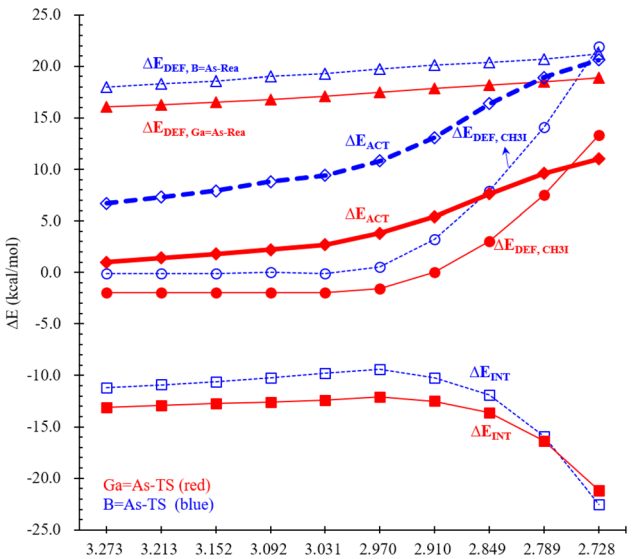

Fig. 11 ASM profiles along the intrinsic reaction coordinate for the 1,3-addition reactions of CH_3I with LB-based imine analogues, **B=N-Rea** (black) and **Tl=N-Rea** (red). All calculations were carried out at the ZORA-M06-2X-D3/TZ2P//M06-2X-D3/def2-TZVP level of theory.

highlight deformation energy as a critical factor that can be strategically modulated to tune the reactivity of main group compounds.

4 Conclusions

In this study, we performed a comprehensive computational investigation on five germylene-stabilized, doubly bonded imine-like molecules with the general formula (L)G13=As–Ge(L) (*i.e.*, **G13=As-Rea**), where L = CH[C(Me)NAr]$_2$ and Ar = 2,6-iPr$_2$C$_6$H$_3$). Theoretical results, particularly those related to their reactivity toward CH_3I, offer significant insights into how the G13=As–Ge framework influences both the stability of the G13=As double bond and its chemical reactivity. These findings lead to the following key conclusions:

1. The EDA analyses reveals that an electron-sharing (triplet–triplet) bonding interaction predominates in both doubly bonded imine analogues, (L)B=As–L$_2$ (**B=As-Rea**) and (L)Al=As–L$_2$ (**Al=As-Rea**), which contain a mixed B–As–Ge or Al–As–Ge bonding framework. However, our computational EDA results suggest that the bonding in the imine-like **Ga=As-Rea** compound can be interpreted either as two mutual dative bonds, (L)Ga ⇆ As–L$_2$, or as an electron-sharing double bond, (L)Ga=As–L$_2$. In contrast, the bonding situations in **In=As-Rea** and **Tl=As-Rea** are best described as donor–acceptor (singlet–singlet) interactions, specifically (L)In ⇆ As–L$_2$ and (L)Tl ⇆ As–L$_2$, rather than covalent electron-sharing bonds.

2. The VB theory predicts that the bond angle ∠G13–As–Ge in (L)G13=As–Ge(L) (*i.e.*, **G13=As-Rea**) compounds is close to 90°, a result that aligns well with the available experimental structural data.[21–39]

3. Our M06-2X computational analysis reveals that, with the exception of the boron–arsenic imine analogue (**B=As-Rea**), the other four heavier imine analogues—**Al=As-Rea**, **Ga=As-Rea**, **In=As-Rea**, and **Tl=As-Rea**—readily undergo 1,3-addition reactions with CH_3I through an intramolecular FLP pathway. Both kinetic and thermodynamic parameters support this conclusion, as illustrated in Fig. 12. These theoretical predictions are consistent with available experimental evidence for the Ga=As-based imine analogue.[39]

4. Our EDA analysis reveals that, in the **G13=As-TS** structure, the interaction between CH_3I and the heavy imine analogues (**G13=As-Rea**) is primarily governed by a donor–acceptor bonding mechanism, characterized by singlet–singlet orbital interactions. This bonding mode contrasts with an electron-

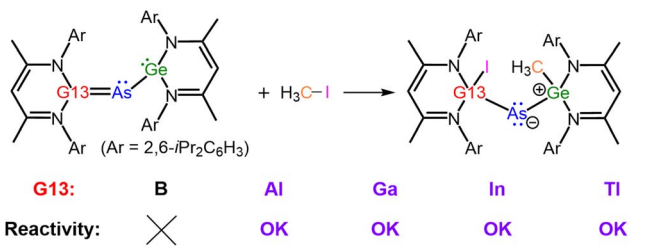

Fig. 12 Computational predictions of 1,3-addition reaction of the heavy imine-like **G13=As-Rea** molecule and CH_3I.

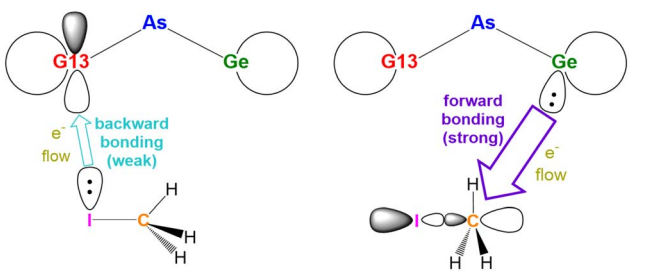

Fig. 13 The donor–acceptor bonding interactions between the heavy imine-like **G13=As-Rea** molecule and CH_3I.

sharing (triplet–triplet) interaction, which contributes negligibly in this context.

5. Computational analyses based on the FMO theory and EDA-NOCV reveal that the predominant bonding interaction in the **G13**=**As-TS** structure arises from electron donation from the lone pair orbital of the Ge center in the **G13**=**As-Rea** molecule to the antibonding σ* orbital of the **H_3C–I** bond in CH_3I. This forward bonding interaction is characterized by the orbital overlap: lone pair (Ge) → σ*(C–I). In addition, a secondary, less significant interaction involves electron donation from the filled σ orbital of the C–I bond in CH_3I to the vacant p–π* orbital on the G13 center of **G13**=**As-Rea**, corresponding to a backward bonding interaction: σ(C–I) → p–π*(G13). These orbital interactions are illustrated schematically in Fig. 13.

6. Our ASM analysis indicates that the activation energy for the 1,3-addition reaction between CH_3I and the heavy imine-like compound **G13**=**As-Rea** is predominantly governed by the deformation energy ($\Delta E_{DEF,G13=As\text{-}Rea}$) of the **G13**=**As-Rea** fragment in the **G13**=**As-TS** transition state. This deformation energy is further attributed to the relativistic effects associated with the heavy G13 central atom in the **G13**=**As-Rea** species, which plays a crucial role in modulating the activation barrier for such 1,3-addition reactions.

7. Our computational results demonstrate that when the transition state (**G13**=**As-TS**) exhibits a more reactant-like character, it is located earlier along the reaction coordinate and corresponds to a lower activation energy. Conversely, when the transition state is more product-like, it appears later along the reaction path and is associated with decreased exergonicity. These trends are in accordance with Hammond's postulate, which relates the structure of the transition state to the kinetics of the reaction.

Author contributions

Zheng-Feng Zhang: literature search, computer calculation of chemical data, graphic drawing and layout, and data collation and discussion. Ming-Der Su: discussion and writing and editing papers.

Conflicts of interest

There are no conflicts to declare.

Data availability

The data supporting this article have been included as part of the supplementary information (SI). Supplementary information is available. See DOI: https://doi.org/10.1039/d5ra07521a.

Acknowledgements

The authors extend their sincere thanks to the National Center for High-Performance Computing of Taiwan for the provision of essential computational resources, which played a pivotal role in advancing this research. Additionally, the authors are grateful for the financial support from the National Science and Technology Council (NSTC), Taiwan. The authors also appreciate the thoughtful comments and helpful suggestions from Reviewers 1 and 2.

References

1 P. P. Power, *Chem. Rev.*, 1999, **99**, 3463–3504.
2 S. Schulz, *Adv. Organomet. Chem.*, 2003, **49**, 225–317.
3 R. C. Fischer and P. P. Power, *Chem. Rev.*, 2010, **110**, 3877–3923.
4 M. A. Malik, M. Afzaal and P. O'Brien, *Chem. Rev.*, 2010, **110**, 4417–4446.
5 A. C. Jones and P. O'Brien, *CVD of Compound Semiconductors, Precursor Synthesis, Development and Application*, VCH, Weinheim, Germany, 1996.
6 A. H. Cowley and R. A. Jones, *Angew. Chem., Int. Ed.*, 1989, **28**, 1208–1215.
7 A. H. Cowley and R. A. Jones, *Polyhedron*, 1994, **13**, 1149–1157.
8 D. A. Atwood, A. H. Cowley, R. A. Jones and M. A. Mardones, *J. Organomet. Chem.*, 1993, **449**, C1–C2.
9 R. J. Jouet, A. P. Purdy, R. L. Well and J. F. Janik, *J. Cluster Sci.*, 2002, **13**, 469–486.
10 A. Y. Timoshkin, *Coord. Chem. Rev.*, 2005, **249**, 2094–2131.
11 T. J. Clark, K. Lee and I. Manners, *Chem.–Eur. J.*, 2006, **12**, 8634–8648.
12 T. B. Marder, *Angew. Chem., Int. Ed.*, 2007, **46**, 8116–8118.
13 H. W. Langmi and G. S. McGrady, *Coord. Chem. Rev.*, 2007, **251**, 925–935.
14 M. Jacoby, *Chem. Eng. News*, 2008, **85**, 61–71.
15 A. Y. Timoshkin and H. F. Schaefer, *J. Phys. Chem. A*, 2008, **112**, 13180–13196.
16 T.-W. Shih, M.-C. Li and M.-D. Su, *Inorg. Chem.*, 2015, **54**, 5154–5161.
17 K. K. Pandey, R. Vishwakarma and S. K. Patidar, *Comput. Theor. Chem.*, 2016, **1076**, 23–31.
18 C. Weetman, *Chem.–Eur. J.*, 2021, **27**, 1941–1954.
19 M. K. Sharma, C. Wölper and S. Schulz, *Dalton Trans.*, 2022, **51**, 1612–1616.
20 F. Dankert and C. Hering-Junghans, *Chem. Commun.*, 2022, **58**, 1242–1262.
21 E. Rivard, W. A. Merrill, J. C. Fettinger and P. P. Power, *Chem. Commun.*, 2006, **42**, 3800–3802.
22 E. Rivard, W. A. Merrill, J. C. Fettinger, R. Wolf, G. H. Spikes and P. P. Power, *Inorg. Chem.*, 2007, **46**, 2971–2978.
23 F. Dahcheh, D. Martin, D. W. Stephan and G. Bertrand, *Angew. Chem., Int. Ed.*, 2014, **53**, 13159–13163.
24 F. Dahcheh, D. W. Stephan and G. Bertrand, *Chem.–Eur. J.*, 2015, **21**, 199–204.
25 H. Braunschweig, W. C. Ewing, K. Geetharani and M. Schäfer, *Angew. Chem., Int. Ed.*, 2015, **54**, 1662–1665.
26 A. N. Price and M. J. Cowley, *Chem.–Eur. J.*, 2016, **22**, 6248–6252.
27 A. N. Price, G. S. Nichol and M. J. Cowley, *Angew. Chem., Int. Ed.*, 2017, **56**, 9953–9957.
28 C. Ganesamoorthy, C. Helling, C. Wölper, W. Frank, E. Bill, G. E. Cutsail and S. Schulz, *Nat. Commun.*, 2018, **9**, 87–94.

29 C. Helling, C. Wölper and S. Schulz, *J. Am. Chem. Soc.*, 2018, **140**, 5053–5056.
30 J. Krüger, C. Ganesamoorthy, L. John, C. Wölper and S. Schulz, *Chem.–Eur. J.*, 2018, **24**, 9157–9164.
31 C. Helling, C. Wölper, Y. Schulte, G. E. Cutsail and S. Schulz, *Inorg. Chem.*, 2019, **58**, 10323–10332.
32 J. Schoening, L. John, C. Wölper and S. Schulz, *Dalton Trans.*, 2019, **48**, 17729–17734.
33 B. Li, C. Wölper, G. Haberhauer and S. Schulz, *Angew. Chem., Int. Ed.*, 2021, **60**, 1986–1991.
34 J. Krüger, C. Wölper and S. Schulz, *Angew. Chem., Int. Ed.*, 2021, **60**, 3572–3575.
35 M. K. Sharma, C. Wölper, G. Haberhauer and S. Schulz, *Angew. Chem., Int. Ed.*, 2021, **60**, 6784–6790.
36 W. Yang, K. E. Krantz, D. A. Dickie, A. Molino, D. J. D. Wilson and R. J. Gilliard Jr, *Angew. Chem., Int. Ed.*, 2020, **59**, 3971–3975.
37 D. W. N. Wilson, J. Feld and J. M. Goicoechea, *Angew. Chem., Int. Ed.*, 2020, **59**, 20914–20918.
38 M. Fischer, S. Nees, T. Kupfer, J. T. Goettel, H. Braunschweig and C. Hering-Junghans, *J. Am. Chem. Soc.*, 2021, **143**, 4106–4111.
39 S. Nees, T. Wellnitz, F. Dankert, M. Härterich, S. Dotzauer, M. Feldt, H. Braunschweig and C. Hering-Junghans, *Angew. Chem., Int. Ed.*, 2023, **62**, e202215838.
40 T. Taeufer, F. Dankert, D. Michalik, J. Pospech, J. Bresien and C. Hering-Junghans, *Chem. Sci.*, 2023, **14**, 3018–3023.
41 A. Koner, B. Morgenstern and D. M. Andrada, *Angew. Chem., Int. Ed.*, 2022, **61**, e202203345.
42 L. S. Szych, J. Bresien, L. Fischer, M. J. Ernst and J. M. Goicoechea, *Chem. Sci.*, 2025, **16**, 7397–7417.
43 Y. Wang, H. S. Karnamkkott, J. Wang, Y. Zhu, M. Zhang, M. Kumari, K. C. Mondal and B. Li, *Inorg. Chem.*, 2025, **64**, 3485–3494.
44 Y. Zhao and D. G. Truhlar, *J. Chem. Theory Comput.*, 2008, **4**, 1849–1868.
45 S. Grimme, J. Antony, S. Ehrlich and H. Krieg, *J. Chem. Phys.*, 2010, **132**, 154104–154122.
46 S. Grimme, S. Ehrlich and L. Goerigk, *J. Comput. Chem.*, 2011, **32**, 1456–1465.
47 D. G. A. Smith, L. A. Burns, K. Patkowski and C. D. Sherrill, *J. Phys. Chem. Lett.*, 2016, **7**, 2197–2203.
48 F. Weigend, *Phys. Chem. Chem. Phys.*, 2006, **8**, 1057–1065.
49 M. J. Frisch, G. W. Trucks, H. B. Schlegel, G. E. Scuseria, M. A. Robb, J. R. Cheeseman, G. Scalmani, V. Barone, G. A. Petersson, H. Nakatsuji, X. Li, M. Caricato, A. V. Marenich, J. Bloino, B. G. Janesko, R. Gomperts, B. Mennucci, H. P. Hratchian, J. V. Ortiz, A. F. Izmaylov, J. L. Sonnenberg, D. Williams-Young, F. Ding, F. Lipparini, F. Egidi, J. Goings, B. Peng, A. Petrone, T. Henderson, D. Ranasinghe, V. G. Zakrzewski, J. Gao, N. Rega, G. Zheng, W. Liang, M. Hada, M. Ehara, K. Toyota, R. Fukuda, J. Hasegawa, M. Ishida, T. Nakajima, Y. Honda, O. Kitao, H. Nakai, T. Vreven, K. Throssell, J. A. Montgomery, Jr., J. E. Peralta, F. Ogliaro, M. J. Bearpark, J. J. Heyd, E. N. Brothers, K. N. Kudin, V. N. Staroverov, T. A. Keith, R. Kobayashi, J. Normand, K. Raghavachari, A. P. Rendell, J. C. Burant, S. S. Iyengar, J. Tomasi, M. Cossi, J. M. Millam, M. Klene, C. Adamo, R. Cammi, J. W. Ochterski, R. L. Martin, K. Morokuma, O. Farkas, J. B. Foresman, and D. J. Fox, *Gaussian 16, Revision C.01*, Gaussian, Inc., Wallingford CT, 2016.
50 R. Kretschmer, D. A. Ruiz, C. E. Moore, A. L. Rheingold and G. Bertrand, *Angew. Chem., Int. Ed.*, 2014, **53**, 8176–8179.
51 M. Soleilhavoup and G. Bertrand, *Acc. Chem. Res.*, 2015, **48**, 256–266.
52 K. Morokuma, *J. Chem. Phys.*, 1971, **55**, 1236–1244.
53 T. Ziegler and A. Rauk, *Theor. Chim. Acta*, 1977, **46**, 1–10.
54 T. Ziegler and A. Rauk, *Inorg. Chem.*, 1979, **18**, 1558–1565.
55 F. M. Bickelhaupt and T. Ziegler, *Organometallics*, 1995, **14**, 2288–2296.
56 *Computer Code ADF2017, SCM, Theoretical Chemistry*, Vrije Universiteit, Amsterdam, The Netherlands, http://www.scm.com.
57 C. Chang, M. Pelissier and Ph. Durand, *Phys. Scr.*, 1986, **34**, 394–404.
58 J.-L. Heullyt, I. Lindgrent, E. Lindrothi, S. Lundqvist and A.-M. Pendrill, *J. Phys., B*, 1986, **19**, 2799–2815.
59 E. van Lenthe and E. J. Baerends, *J. Comput. Chem.*, 2003, **24**, 1142–1156.
60 M. Mitoraj and A. Michalak, *J. Mol. Model.*, 2007, **13**, 347–355.
61 M. Mitoraj and A. Michalak, *Organometallics*, 2007, **26**, 6576–6580.
62 A. Michalak, M. Mitoraj and T. Ziegler, *J. Phys. Chem. A*, 2008, **112**, 1933–1939.
63 M. Mitoraj, A. Michalak and T. Ziegler, *J. Chem. Theory Comput.*, 2009, **5**, 962–975.
64 W.-J. van Zeist and F. M. Bickelhaupt, *Org. Biomol. Chem.*, 2010, **8**, 3118–3127.
65 I. Fernández and F. M. Bickelhaupt, *Chem. Soc. Rev.*, 2014, **43**, 4953–4967.
66 I. Fernández, *Phys. Chem. Chem. Phys.*, 2014, **16**, 7662–7671.
67 L. P. Wolters and F. M. Bickelhaupt, *Wiley Interdiscip. Rev.: Comput. Mol. Sci.*, 2015, **5**, 324–343.
68 I. Fernández, in *Discovering the Future of Molecular Sciences*, ed. B. Pignataro, Wiley-VCH, Weinheim, 2014, pp. 165–187.
69 D. H. Ess and K. N. Houk, *J. Am. Chem. Soc.*, 2007, **129**, 10646–10647.
70 D. H. Ess and K. N. Houk, *J. Am. Chem. Soc.*, 2008, **130**, 10187–10198.
71 D. H. Ess, G. O. Jones and K. N. Houk, *Org. Lett.*, 2008, **10**, 1633–1636.
72 L. Zhao, S. Pan, N. Holzmann, P. Schwerdtfeger and G. Frenking, *Chem. Rev.*, 2019, **119**, 8781–8845.
73 R. J. Boyd and M. Yanez, *Comprehensive Computational Chemistry*, Elsevier, 2023, vol. 2, pp. 322–361.
74 C. Mohapatra, S. Kundu, R. Herbst-Irmer, D. Stalke, D. M. Andrada, G. Frenking and H. W. Roesky, *J. Am. Chem. Soc.*, 2016, **138**, 10429–10432.
75 E. D. Glendening, J. K. Badenhoop, A. E. Reed, J. E. Carpenter, J. A. Bohmann, C. M. Morales, C. R. Landis and F. Weinhold, *NBO 6.0, Theoretical Chemistry Institute*,

University of Wisconsin, Madison, WI, 2013, http://nbo6.chem.wisc.edu/.
76 Further work along this line is in progress and will be published shortly.
77 P. Pyykkö and J. P. Desclaux, *Acc. Chem. Res.*, 1979, **12**, 276–281.
78 W. Kutzelnigg, *Angew. Chem., Int. Ed.*, 1984, **23**, 272–295.
79 P. Pyykkö, *Chem. Rev.*, 1988, **88**, 563–594.
80 P. Pyykkö, *Chem. Rev.*, 1997, **97**, 597–636.
81 Z.-F. Zhang, M.-C. Yang and M.-D. Su, *Inorg. Chem.*, 2021, **60**, 15253–15269.
82 K. N. Houk, *Acc. Chem. Res.*, 1975, **8**, 361–369.
83 K. H. Dötz and J. Stendel Jr, *Chem. Rev.*, 2009, **109**, 3227–3274.
84 R. H. Crabtree, *The Organometallic Chemistry of the Transition Metals*, Wiley, New York, 4th edn, 2005, pp. 310–311.
85 P. Jerabek, P. Schwerdtfeger and G. Frenking, *J. Comput. Chem.*, 2019, **40**, 247–264.
86 G. S. Hammond, *J. Am. Chem. Soc.*, 1955, **77**, 334–338.